PCCP

RSC Publishing

PAPER

View Article Online
View Journal | View Issue

Infrared biosensors based on graphene plasmonics: modeling†

Cite this: *Phys. Chem. Chem. Phys.*, 2013, **15**, 17118

Yuan Zhao,[a] Xiang Hu,[b] Guanxiong Chen,[a] Xuanru Zhang,[b] Ziqi Tan,[a] Junhua Chen,[a] Rodney S. Ruoff,[c] Yanwu Zhu*[a] and Yalin Lu*[abd]

Received 8th May 2013,
Accepted 5th August 2013

DOI: 10.1039/c3cp51952j

www.rsc.org/pccp

We propose a biosensor by exploiting localized plasmons in graphene and biomolecule adsorption on it. Numerical simulations demonstrate that the sensitivity of such a device can achieve a high value of up to 1697 nm/RIU (refractive index unit) when the wavelength shift at the plasmon resonance is detected. The transparent substrate supporting graphene can be chosen potentially from a wide range of materials including insulators, semiconductors, polymers, and gels. The plasmon resonance wavelength can be tuned with electrostatic doping and/or structure modulation of graphene. Furthermore, the device works in a wide angle range of incident light since the transverse magnetic (TM) polarization is independent of incident angles.

1. Introduction

Plasmons have sparked a wealth of research interest in a wide range of systems from metallic films[1] to metallic nanoparticles,[2] carbon molecules[3] and recently graphene.[4] The collective oscillations of conducting electrons in these systems may bring about plasmon resonance when interacting with incident light. These plasmonic structures concentrate light into a sub-wavelength scale and enhance the electric field intensity by orders of magnitude higher than the signal from fluorophores or quantum dots, thus leading to a broad range of applications such as sub-wavelength wave-guiding,[5–8] surface-enhanced Raman spectroscopy,[9] biomedicine[10] and particularly related to our work here, plasmonic biosensing.[11–15]

A basic plasmonic biosensor detects a change in optical signals (*e.g.* the shift in resonant wavelength and/or the intensity change at a certain wavelength) when the detecting platform interacts with biomolecules.[16] Such a change may be sensitive to the adsorption of biomolecules. Plasmonic biosensing has been investigated for monitoring food safety,[17] for immunoassay,[18] and for medical diagnostics in a label-free manner.[16,19,20] In the last 20 years, significant efforts have been devoted to the fabrication of plasmonic nanostructures, such as gold nanodisks, nanorings/disks, nanocrosses, nanoshells, 'bow tie' structures, and so on.[21–24] However, the fine control of structure and morphology in such nanostructures remains a challenge. Moreover, commonly-used metal gold does not adsorb biomolecules ideally due to its intrinsical hydrophobicity and high surface inertness.[13,14,25] Silver nanostructures covered by an anti-oxidation layer have been tested for biosensing, while further optimization for improved performances is needed.[12–15] One other shortcoming for metals when being used in infrared plasmonic biosensing is the relatively weak field confinement on the metal surface, leading to a limited sensitivity.[26] Apart from metal-based plasmonic biosensors, semiconductors have been used in plasmonic sensors in terahertz frequency ranges due to the small values of permittivity.[27,28]

Recently, graphene has attracted intensive interest in fields including physics, chemistry, materials science, and biology.[29–34] It has been shown that graphene itself supports plasmons both in mid- and far-infrared regions with tunable Fermi energy levels.[35,36] Graphene plasmonic nanostructures are also emerging and suggest a few potential applications.[4,37,38] It was reported that the confinement of plasmons in graphene is stronger than that in metals due to the two-dimensional nature of collective excitations in graphene and shorter plasmon wavelength compared to the excitation wavelength.[38,39] The strong adsorption of biomolecules on graphene reported was considered due to the π-stacking interaction between biomolecules and graphene, and possibly

[a] *Department of Materials Science and Engineering and CAS Key Laboratory of Materials for Energy Conversion, University of Science and Technology of China, 96 Jin Zhai Rd, Hefei 230026, China. E-mail: zhuyanwu@ustc.edu.cn, yllu@ustc.edu.cn*

[b] *Advanced Applied Research Center, Hefei National Laboratory for Physical Sciences at the Microscale, University of Science and Technology of China, 96 Jin Zhai Rd, Hefei 230026, China*

[c] *Department of Mechanical Engineering and the Materials Science and Engineering Program, The University of Texas at Austin, One University Station C2200, Austin, TX 78712, USA*

[d] *Laser Optics Research Center, Physics Department, United States Air Force Academy, CO 80840, USA*

† Electronic supplementary information (ESI) available. See DOI: 10.1039/c3cp51952j

the high surface to volume ratio of graphene, further benefiting biosensing.[12–14,40] In previous studies on graphene biosensing, the graphene was decorated with metal nanostructures to excite plasmons.[12,15] Tuning the plasmonic properties of graphene for optimized sensing performance has been theoretically attempted.[26] A biosensor combining the merits of graphene plasmons and the adsorption of biomolecules on graphene may be useful in future biosensing applications.

In this work, we propose a simple yet versatile graphene plasmonic structure that uses graphene plasmons in a biosensor. Based on a modeled configuration, narrow-band transmission spectra in the mid-infrared region have been obtained to detect the molecules adsorbed on graphene. The proposed device can achieve a sensitivity of up to 1697 nm/RIU (refractive index unit) when being used for sensing a few types of biomolecules. The sensing sensitivity and accuracy are optimized by tuning the substrate materials, geometric parameters, and the Fermi energy levels of graphene. More modifications of the structure by using a rough substrate or adding a reflection mirror are also investigated.

2. Structure and methods

The structure of a graphene plasmonic biosensor is schematically illustrated in Fig. 1. The graphene film is patterned into periodic arrays of nanoribbons sitting on a transparent substrate. The sensing medium containing biomolecules is placed in direct contact with the graphene nanoribbon arrays. Light irradiates the device from the top with transverse magnetic (TM) polarization (normal incidence). The wavelength at transmission resonance can be expressed as:[4,39,41]

$$\lambda_p = \mathrm{Re}\left(\frac{2ic\eta\varepsilon_0(\varepsilon_{r1}+\varepsilon_{r2})w}{\sigma}\right) \quad (1)$$

where, λ_p is the resonance wavelength of the graphene plasmons, c the velocity of light in the vacuum, w the nanoribbon width, ε_0 the permittivity of vacuum, ε_{r1} and ε_{r2} the dielectric constants of the materials above and under the graphene film, respectively,

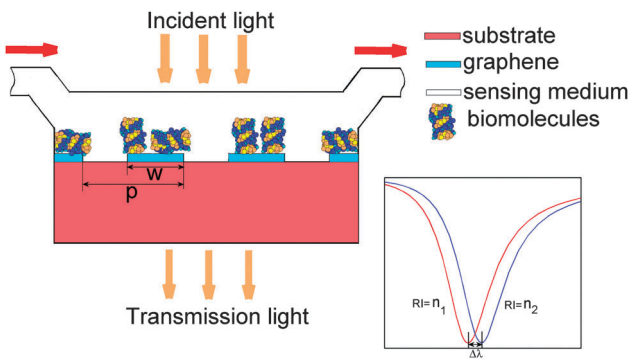

Fig. 1 Schematic of the graphene plasmonic biosensor. The graphene nanoribbons (period p, nanoribbon width w) sitting on a substrate are in direct contact with biomolecules in sensing medium. The resonance wavelength has a shift when refractive index (RI) of biomolecules is changed.

σ the conductivity of graphene and η a dimensionless constant standing for the electrodynamic responses of the nanoribbon array (see ESI† for details).[4] As the AC (alternating current) conductivity is a function of the graphene Fermi energy level (E_F) and the wavelength of incident light, the resonance wavelength can be approximated as the expression below when the intraband transitions are considered[39,41] (ESI†)

$$\lambda_p \cong \frac{2\pi\hbar c}{e}\sqrt{\frac{\eta\varepsilon_0(\varepsilon_{r1}+\varepsilon_{r2})w}{E_F}} \quad (2)$$

Eqn (2) suggests that the resonance wavelength λ_p shifts with a change in dielectric constant ε_{r1} of the sensing medium. In this way, the existence (and possible transformation) of biomolecules can be detected by measuring the shift in the resonance wavelength because ε_{r1} is affected by the adsorption of biomolecules on graphene. The refractive index (RI) range of the sensing media has been selected to cover some frequently studied biomolecules such as human g-immunoglobulin (IgG, RI: 1.41),[42] human serum albumin (HSA, RI: 1.445),[42] single-stranded DNA (ss-DNA, RI: 1.462) and double-stranded DNA (ds-DNA, RI: 1.53).[13]

The simulations were performed using Comsol Multiphysics (COMSOL 3.5a), which implements the finite element method (FEM) to solve Maxwell's equations and is a widely accepted method for modeling optics[43–45] (see ESI† for details). The graphene film was modeled as a thin layer with a thickness of 0.34 nm, as in ref. 41 and 46. The mobility of graphene ribbons is considered close to that in their large-area counterparts when the nanoribbon width is above 50 nm.[47–49] By treating the graphene film as a uniform dielectric layer, the results did not change when setting the thickness to a different value. If considering graphene with stacked layers rather than a single layer, *ab initio* calculations could also be done.[50,51]

To evaluate the performance of the plasmonic biosensor, two main parameters,[16,52] namely sensitivity and detection accuracy, were calculated. The sensitivity (S) is defined as the ratio of the shift in resonance wavelength ($\Delta\lambda_p$) to the RI change in the sensing medium (Δn_s, $n_s = \varepsilon_{r1}^{(1/2)}$), *i.e.*,

$$S = \frac{\Delta\lambda_p}{\Delta n_s} = \frac{2\pi\eta\hbar c}{e}\sqrt{\frac{\varepsilon_0 w}{E_F}}\frac{n_s}{\sqrt{(n_s^2+\varepsilon_{r2})}} \quad (3)$$

The transmission intensity change with a fixed incident wavelength can also be used to detect the RI changes in biomolecules (see ESI† for details). The detection accuracy (D) is defined as the reciprocal of the full width at half-maximum (FWHM) of the resonance spectrum,

$$D = \frac{1}{\mathrm{FWHM}} \quad (4)$$

Hence, to achieve both high sensitivity and high detection accuracy, a plasmonic resonance curve should have a large spectral shift with the same RI change and a narrow line width, respectively. The figure of merit (FOM) is defined as

$$\mathrm{FOM} = S \times D \quad (5)$$

3. Results and discussion

3.1 Effects of substrate dielectric constants

Recent studies have shown that large-area graphene films can be synthesized on metals and then transferred to other substrates.[53–55] To select a proper substrate, the transmission spectrum was simulated for substrates with various dielectric constants (Fig. 2a). The Fermi energy level E_F was selected to be 0.2 eV (as discussed in ESI†); the period and the nanoribbon width were p = 400 nm and w = 200 nm, respectively. As predicted in eqn (2), the resonance shifts to a longer wavelength with an increase of dielectric constant. Simultaneously, the FWHM becomes larger, indicating a decreased detection accuracy (Fig. 2c), which is in agreement with the results reported in ref. 56. A few commonly-used materials such as MgF_2,[57] poly(methyl methacrylate) (PMMA),[58] poly(styrene) (PS),[58] ion gel,[4] SiO_2,[4] SiC[59] and Si[59] have been evaluated.

The sensitivity for these substrates is summarized in Fig. 2b. The highest sensitivity is 1697 nm/RIU for a low RI substrate, MgF_2. This high sensitivity can be explained by the fact that the graphene plasmon wavelength is much shorter than the excitation wavelength, resulting in a high field localization and thus a stronger light–biomolecule interaction.[38,41,56] In addition, the low group velocity of plasmonic waves (~c/100) allows for longer interaction between biomolecules and light as waves propagate slowly through the water solution.[41,46] The sensitivity calculated is 1382, 1131, 1349, 1281, 1218, 1150, 754 nm/RIU for PMMA, PS, ion gel, SiO_2, SiC or Si substrates, respectively (see ESI† for the calculation details), all comparable to or higher than the sensitivity of current excellent metal-based plasmonic biosensors.[21–23] The monotonic decrease in sensitivity with increasing dielectric constant was considered to be caused by the increased damping of plasmon oscillations and smaller field localization.[60,61] The decrease in detection accuracy (Fig. 2c) when increasing the dielectric constant is attributed to increased losses and decreased field localization.[60] Substrates with lower dielectric constants gave higher FOM values, as shown in Fig. 2d. Due to its relatively high FOM and low cost, PMMA has been considered to be the substrate for the following analyses.

3.2 Effects of graphene plasmonic structures

Plasmonic resonance with wavelengths ranging from mid-infrared to terahertz regions was reported in graphene arrays by tuning the structure parameters.[4,56,62] The effect of the graphene structure on the biosensing was investigated and the results are shown in Fig. 3. Fig. 3a shows the transmission spectrum as a function of graphene nanoribbon width w with period p fixed at 400 nm. It can be seen that the resonance minimum shifts to a longer wavelength with increasing width, consistent

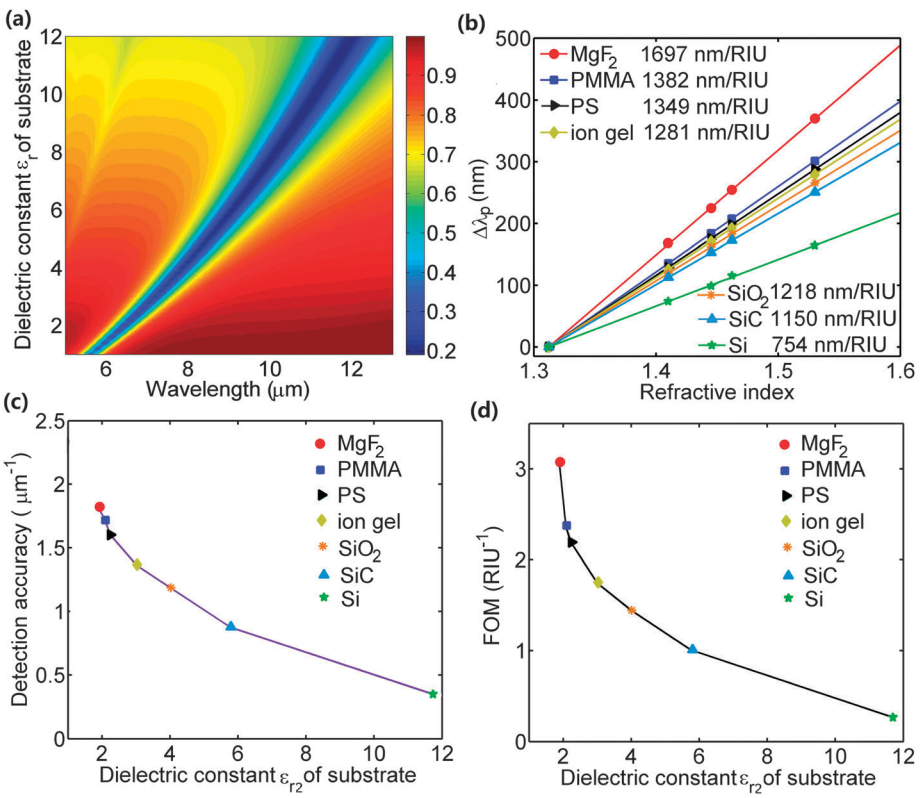

Fig. 2 Graphene plasmonic biosensing with varying dielectric constant of transparent substrates. (a) Simulated normal-incidence transmittance mapping with varying dielectric constant ε_{r2} of substrates and incident wavelength when E_F = 0.2 eV and $p = 2w$ = 400 nm. (b)–(d) Shows (b) sensitivity, (c) detection accuracy and (d) FOM for seven commonly-used substrates with different dielectric constants, respectively. The sensing medium shown in (b) (from left to right) changes from water (n = 1.312) to IgG (human g-immunoglobulin, n = 1.41), HSA (human serum albumin, n = 1.445), ss-DNA (single-stranded DNA, n = 1.462), and to ds-DNA (double-stranded DNA, n = 1.53) in water solutions. Lines are linear fittings to the data.

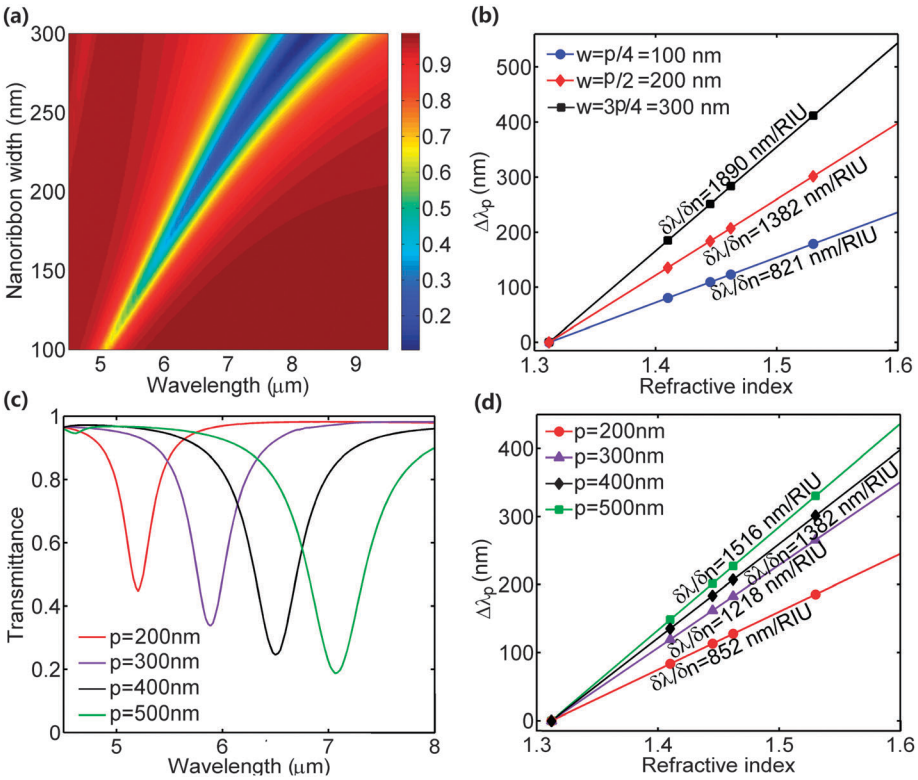

Fig. 3 Graphene plasmonic biosensing for graphene on a PMMA substrate with varying structure parameters. (a) Simulated normal-incidence transmission spectra with varying nanoribbon widths and incident wavelengths and (b) calculated sensitivity when the nanoribbon width is 0.25p, 0.5p, 0.75p, respectively, for E_F = 0.2 eV and p = 400 nm. (c) The transmittance spectra and (d) sensitivity for periods of 200, 300, 400 and 500 nm, respectively, when E_F = 0.2 eV and nanoribbon width to be 1/2 period. The symbols (from left to right) in (b) and (d) denote the sensing medium changes from water to IgG, HSA, ss-DNA, and to ds-DNA in water solutions. Lines are linear fittings to the data.

with eqn (2) and also in agreement with the trend reported in ref. 56. The line width broadens for wider nanoribbons, due to decreased field confinement, increased damping and loss arising from the increased real part of the graphene conductivity with larger resonance wavelength.[15,61] The numerical calculation yields a relationship of the resonance wavelength λ_p and nanoribbon width w as $\lambda_p/w^{1/2} \approx 0.015\ [m]^{1/2}$, which agrees well with the prediction based on eqn (2) (explained in ESI†). As examples, nanoribbon widths of 0.25p (100 nm), 0.5p (200 nm), and 0.75p (300 nm) were modeled and the sensitivity obtained is 821, 1382, and 1890 nm/RIU, respectively (Fig. 3b). The corresponding FOM is 2.17, 2.37, and 1.49 RIU^{-1}, respectively.

The effect of the period of the graphene nanoribbon arrays was studied by fixing the value of w/p to be 1/2. It can be seen from Fig. 3c that the resonance shifts to a longer wavelength and the resonance curve broadens with increasing period,

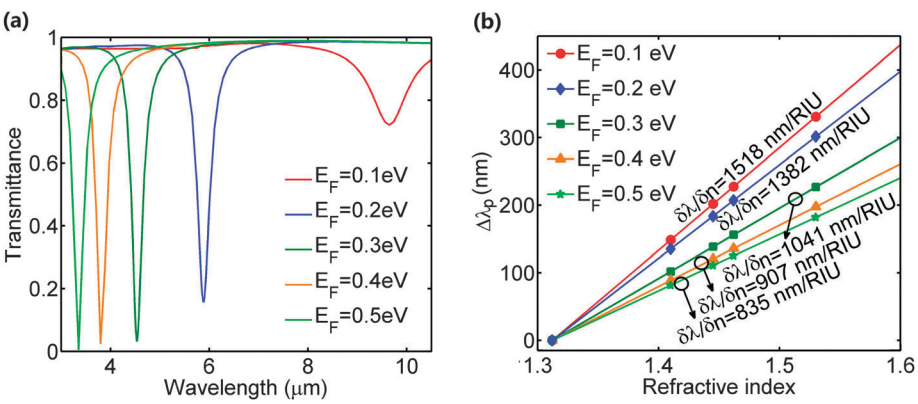

Fig. 4 Graphene plasmonic biosensing with varying Fermi energy levels E_F of graphene. (a) Simulated normal-incidence transmission spectra and (b) corresponding sensitivity for Fermi energy levels E_F of 0.1, 0.2, 0.3, 0.4 and 0.5 eV, respectively, when p = 2w = 300 nm. The symbols (from left to right) on each line in (b) denote the sensing medium changes from water to IgG, HSA, ss-DNA, and to ds-DNA in water solutions. Lines are linear fittings to the data.

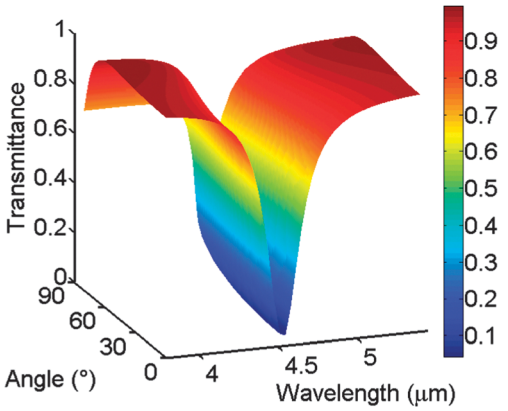

Fig. 5 The simulated angular dispersions of the transmittance for TM configurations when E_F = 0.3 eV and $p = 2w$ = 300 nm.

leading to a decreased detection accuracy. However, the structure with larger periods demonstrates much higher sensitivity for the same RI change (Fig. 3d). Such a result is consistent with eqn (3), in which the variation tendency is the same when changing graphene nanoribbon width w, as discussed above for $p = 2w$ (eqn (2); see ESI† for details). The FOM is 2.71, 2.82, 2.37, and 2.27 RIU^{-1} for a period of 200, 300, 400, and 500 nm, respectively. For the range studied, a period p of 300 nm and a nanoribbon width w of 150 nm have given the highest FOM value. These features were used for the following study.

3.3 Effects of electronic tuning of graphene plasmons

One unique property of plasmonics in graphene is the tuning capability of the nanoscale optical field.[4,41,46,63] Graphene's complex conductivity ($\sigma = \sigma_r + i\sigma_i$) is sensitive to the incident wavelength λ, carrier relaxation time τ, temperature T, and Fermi energy level E_F (see ESI† for details).[4,46,64] The Fermi energy level E_F can be tuned by gate voltage, electric field, magnetic field, or chemical doping.[4,65–67] The plasmon spectra can be modulated through such means in a wide wavelength range from near-infrared to terahertz.[41]

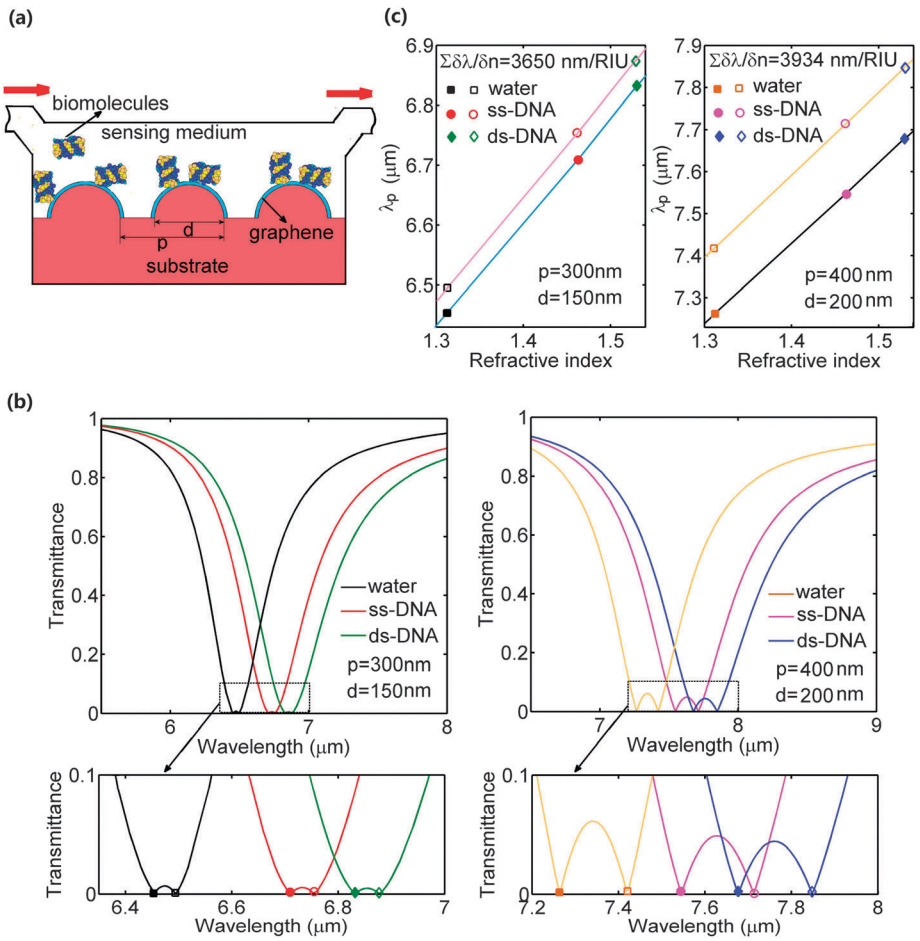

Fig. 6 (a) Schematic of a graphene plasmonic biosensor with a raised half cylinder substrate (period p, diameter d). The graphene layer sitting on the top of the raised half cylinder substrate is in direct contact with biomolecules in sensing medium. (b) Simulated normal-incidence transmission spectra when changing the sensing medium from water to ss-DNA, and to ds-DNA for periods of 300 nm and 400 nm, respectively. The spectra marked by box were zoomed in and shown in the bottom figures. (c) The resonance wavelength λ_p *versus* sensing medium RI curve in a range covering water, ss-DNA and ds-DNA. Solid and hollow symbols stand for the first and second dips, respectively, and lines are linear fittings to the data, giving a summing sensitivity of 3650 nm/RIU and 3934 nm/RIU for periods of 300 nm and 400 nm, respectively.

The transmission spectra shown in Fig. 4a confirm the expected effect of changing the Fermi energy level E_F. The resonance wavelength has a blue shift and the line width gets narrower with increasing E_F. As a result, the accuracy increases monotonically with increasing E_F, presumably due to decreased plasmon damping for higher carrier densities.[38] However, higher E_F of graphene means lower sensitivity for the same RI change (see ESI† for details). The FOM is 1.57, 2.82, 3.93, 3.46, and 3.24 RIU^{-1} for E_F of 0.1, 0.2, 0.3, 0.4, and 0.5 eV, respectively. Furthermore, we have studied the effect of carrier mobility of graphene (see ESI† for more details). The sensitivity does not decrease when the carrier mobility of graphene reduces from 10 000 to 1000 $cm^2\ V^{-1}\ s^{-1}$.

3.4 Effects of incident angles of light

The effect of incident angles on transmittance for TM polarization was investigated and the results are shown in Fig. 5. The resonance minimum is nearly independent of the incident angle. Such a result is attributed to the fact that the magnetic field direction of the TM-polarized incident light does not change with the angle.[23]

3.5 Effects of rough substrates

Graphene allows bending or deformation of flexible substrates such as polymers.[68,69] The influence of surface roughness for a PMMA substrate was investigated. Fig. 6a shows a PMMA substrate with arrays of half cylinders each with a diameter d and a period $p = 2d$. The graphene covers the raised surface of each half cylinder only. The strain calculated is 0.5% or 0.67% for p = 300 nm or p = 400 nm, respectively, when assuming the thickness of graphene as 1 nm. The mobility of graphene in such a case is presumably not changed by the surface roughness of substrates as it can remain relatively constant with a strain of up to 1.75%.[70] The transmission spectra for periods of 300 nm and 400 nm are shown in Fig. 6b; the resonance wavelength shows a red shift compared to the flat substrate with the same period and Fermi energy level, due to an effectively larger graphene nanoribbon width. The plasmon resonance has two transmission minima with each corresponding to a tip in the horizontal and the vertical direction for the raised surface of a half cylinder.[71–73] The 'double dips' were detected and summed to obtain the sensitivity (*i.e.* $\sum \delta\lambda/\delta n$). Fig. 6c shows that the sensitivity can reach a high value of up to 3650 or 3934 nm/RIU for a period of 300 or 400 nm, respectively. Correspondingly, the FOM is 5.93 or 4.95 RIU^{-1}, higher than 2.82 or 2.37 RIU^{-1} for the flat substrate graphene nanoribbon array, respectively.

4. Conclusions

In conclusion, an infrared graphene plasmonic biosensor has been proposed by incorporating graphene plasmons into selective adsorption of biomolecules on the graphene. Our simulations have shown that the interaction between sensing medium (containing biomolecules) and incident optical fields is strong. High sensitivity values of up to 1697 nm/RIU have been achieved when the wavelength shift in the plasmon resonance is detected. The effects of dielectric constants of the transparent substrates, graphene Fermi levels and pattern structures have been studied in detail to optimize the sensitivity and accuracy. In addition, we have demonstrated that the device can work in a wide angle range of incident light or on rough substrates. Furthermore, such a biosensor also works in a reflection structure by using the shift of nearly perfect absorption spectra (see ESI† for more details). These proposed biosensing strategies may be useful for developing simple biosensing devices based on graphene plasmonics.

Acknowledgements

The authors appreciate the financial support from the National Basic Research Program of China (2012CB922001). Y. Zhu thanks support from China Government 1000 Plan Talent Program, China MOE NCET Program and USTC Startup. Y. Lu thanks support from the US Air Force Office of Scientific Research (AFOSR) and DTRA (HDTRA 12221).

Notes and references

1 R. H. Ritchie, *Phys. Rev.*, 1957, **106**, 874–881.
2 V. Myroshnychenko, J. Rodriguez-Fernandez, I. Pastoriza-Santos, A. M. Funston, C. Novo, P. Mulvaney, L. M. Liz-Marzan and F. J. Garcia de Abajo, *Chem. Soc. Rev.*, 2008, **37**, 1792–1805.
3 M. Kociak, L. Henrard, O. Stephan, K. Suenaga and C. Colliex, *Phys. Rev. B: Condens. Matter Mater. Phys.*, 2000, **61**, 13936–13944.
4 L. Ju, B. Geng, J. Horng, C. Girit, M. Martin, Z. Hao, H. A. Bechtel, X. Liang, A. Zettl, Y. R. Shen and F. Wang, *Nat. Nanotechnol.*, 2011, **6**, 630–634.
5 S. Lal, S. Link and N. J. Halas, *Nat. Photonics*, 2007, **1**, 641–648.
6 M. T. Hill, M. Marell, E. S. P. Leong, B. Smalbrugge, Y. Zhu, M. Sun, P. J. van Veldhoven, E. J. Geluk, F. Karouta, Y.-S. Oei, R. Notzel, C.-Z. Ning and M. K. Smit, *Opt. Express*, 2009, **17**, 11107–11112.
7 L. Liu, Z. Han and S. He, *Opt. Express*, 2005, **13**, 6645–6650.
8 W. L. Barnes, A. Dereux and T. W. Ebbesen, *Nature*, 2003, **424**, 824–830.
9 M. Moskovits, *Rev. Mod. Phys.*, 1985, **57**, 783–826.
10 H. Liao, C. L. Nehl and J. H. Hafner, *Nanomedicine*, 2006, **1**, 201–208.
11 J. N. Anker, W. P. Hall, O. Lyandres, N. C. Shah, J. Zhao and R. P. Van Duyne, *Nat. Mater.*, 2008, **7**, 442–453.
12 E. Wijaya, N. Maalouli, R. Boukherroub, S. Szunerits and J. P. Vilcot, *Proc. SPIE*, 2012, 84240R.
13 S. H. Choi, Y. L. Kim and K. M. Byun, *Opt. Express*, 2011, **19**, 458–466.
14 L. Wu, H. S. Chu, W. S. Koh and E. P. Li, *Opt. Express*, 2010, **18**, 14395–14400.
15 J. C. Reed, H. Zhu, A. Y. Zhu, C. Li and E. Cubukcu, *Nano Lett.*, 2012, **12**, 4090–4094.

16 S. Szunerits and R. Boukherroub, *Chem. Commun.*, 2012, **48**, 8999–9010.
17 M. J. Linman, K. Sugerman and Q. Cheng, *Sens. Actuators, B*, 2010, **145**, 613–619.
18 S. D. Mazumdar, B. Barlen, P. Kaempfer and M. Keusgen, *Biosens. Bioelectron.*, 2010, **25**, 967–971.
19 E. Wijaya, C. Lenaerts, S. Maricot, J. Hastanin, S. Habraken, J.-P. Vilcot, R. Boukherroub and S. Szunerits, *Curr. Opin. Solid State Mater. Sci.*, 2011, **15**, 208–224.
20 V. Chabot, C. M. Cuerrier, E. Escher, V. Aimez, M. Grandbois and P. G. Charette, *Biosens. Bioelectron.*, 2009, **24**, 1667–1673.
21 A. E. Cetin and H. Altug, *ACS Nano*, 2012, **6**, 9989–9995.
22 N. Verellen, P. Van Dorpe, C. J. Huang, K. Lodewijks, G. A. E. Vandenbosch, L. Lagae and V. V. Moshchalkov, *Nano Lett.*, 2011, **11**, 391–397.
23 N. Liu, M. Mesch, T. Weiss, M. Hentschel and H. Giessen, *Nano Lett.*, 2010, **10**, 2342–2348.
24 J. B. Lassiter, J. Aizpurua, L. I. Hernandez, D. W. Brandl, I. Romero, S. Lal, J. H. Hafner, P. Nordlander and N. J. Halas, *Nano Lett.*, 2008, **8**, 1212–1218.
25 Z.-C. Xing, Y. Chang and I.-K. Kang, *Sci. Technol. Adv. Mater.*, 2010, **11**, 014101.
26 B. Vasic, G. Isic and R. Gajic, *J. Appl. Phys.*, 2013, **113**, 013110.
27 A. Berrier, R. Ulbricht, M. Bonn and J. G. Rivas, *Opt. Express*, 2010, **18**, 23226–23235.
28 A. Berrier, P. Albella, M. A. Poyli, R. Ulbricht, M. Bonn, J. Aizpurua and J. G. Rivas, *Opt. Express*, 2012, **20**, 5052–5060.
29 A. J. Patil, J. L. Vickery, T. B. Scott and S. Mann, *Adv. Mater.*, 2009, **21**, 3159–3164.
30 A. H. C. Neto, F. Guinea, N. M. R. Peres, K. S. Novoselov and A. K. Geim, *Rev. Mod. Phys.*, 2009, **81**, 109–162.
31 A. K. Geim and K. S. Novoselov, *Nat. Mater.*, 2007, **6**, 183–191.
32 Y. B. Zhang, Y. W. Tan, H. L. Stormer and P. Kim, *Nature*, 2005, **438**, 201–204.
33 K. S. Novoselov, A. K. Geim, S. V. Morozov, D. Jiang, Y. Zhang, S. V. Dubonos, I. V. Grigorieva and A. A. Firsov, *Science*, 2004, **306**, 666–669.
34 C. Berger, Z. Song, X. Li, X. Wu, N. Brown, C. Naud, D. Mayou, T. Li, J. Hass, A. N. Marchenkov, E. H. Conrad, P. N. First and W. A. de Heer, *Science*, 2006, **312**, 1191–1196.
35 H. Yan, X. Li, B. Chandra, G. Tulevski, Y. Wu, M. Freitag, W. Zhu, P. Avouris and F. Xia, *Nat. Nanotechnol.*, 2012, **7**, 330–334.
36 V. W. Brar, M. S. Jang, M. Sherrott, J. J. Lopez and H. A. Atwater, *Nano Lett.*, 2013, **8**, 7806–7813.
37 Z. Fei, A. S. Rodin, G. O. Andreev, W. Bao, A. S. McLeod, M. Wagner, L. M. Zhang, Z. Zhao, M. Thiemens, G. Dominguez, M. M. Fogler, A. H. C. Neto, C. N. Lau, F. Keilmann and D. N. Basov, *Nature*, 2012, **487**, 82–85.
38 J. Chen, M. Badioli, P. Alonso-Gonzalez, S. Thongrattanasiri, F. Huth, J. Osmond, M. Spasenovic, A. Centeno, A. Pesquera, P. Godignon, A. Zurutuza Elorza, N. Camara, F. Javier Garcia de Abajo, R. Hillenbrand and F. H. L. Koppens, *Nature*, 2012, **487**, 77–81.
39 F. H. L. Koppens, D. E. Chang and F. J. G. de Abajo, *Nano Lett.*, 2011, **11**, 3370–3377.
40 C.-H. Lu, H.-H. Yang, C.-L. Zhu, X. Chen and G.-N. Chen, *Angew. Chem., Int. Ed.*, 2009, **48**, 4785–4787.
41 W. Gao, J. Shu, C. Qiu and Q. Xu, *ACS Nano*, 2012, **6**, 7806–7813.
42 J. Voros, *Biophys. J.*, 2004, **87**, 553–561.
43 B. Yun, G. Hu and Y. Cui, *Opt. Express*, 2009, **17**, 3610–3618.
44 A. V. Krasavin and A. V. Zayats, *Phys. Rev. B: Condens. Matter Mater. Phys.*, 2008, **78**, 045425.
45 T. Holmgaard and S. I. Bozhevolnyi, *Phys. Rev. B: Condens. Matter Mater. Phys.*, 2007, **75**, 245405.
46 J. Christensen, A. Manjavacas, S. Thongrattanasiri, F. H. L. Koppens and F. Javier Garcia de Abajo, *ACS Nano*, 2012, **6**, 431–440.
47 F. Schwierz, *Nat. Nanotechnol.*, 2010, **5**, 487–496.
48 M. Bresciani, P. Palestri, D. Esseni, L. Selmi, *Proceedings of the, 39th, European olid-State Device Research Conference. ESSDERC 2009*, 2009, pp. 480–483.
49 N. O. Weiss, H. Zhou, L. Liao, Y. Liu, S. Jiang, Y. Huang and X. Duan, *Adv. Mater.*, 2012, **24**, 5782–5825.
50 E. K. Yu, D. A. Stewart and S. Tiwari, *Phys. Rev. B: Condens. Matter Mater. Phys.*, 2008, **77**, 195406.
51 P. V. Avramov, S. Sakai, S. Entani, Y. Matsumoto and H. Naramoto, *Chem. Phys. Lett.*, 2011, **508**, 86–89.
52 P. K. Maharana and R. Jha, *Sens. Actuators, B*, 2012, **169**, 161–166.
53 Y. Lee, S. Bae, H. Jang, S. Jang, S.-E. Zhu, S. H. Sim, Y. I. Song, B. H. Hong and J.-H. Ahn, *Nano Lett.*, 2010, **10**, 490–493.
54 X. Li, W. Cai, J. An, S. Kim, J. Nah, D. Yang, R. Piner, A. Velamakanni, I. Jung, E. Tutuc, S. K. Banerjee, L. Colombo and R. S. Ruoff, *Science*, 2009, **324**, 1312–1314.
55 K. S. Kim, Y. Zhao, H. Jang, S. Y. Lee, J. M. Kim, K. S. Kim, J.-H. Ahn, P. Kim, J.-Y. Choi and B. H. Hong, *Nature*, 2009, **457**, 706–710.
56 A. Y. Nikitin, F. Guinea, F. J. Garcia-Vidal and L. Martin-Moreno, *Phys. Rev. B: Condens. Matter Mater. Phys.*, 2012, **85**, 081405.
57 J. M. Siqueiros, R. Machorro and L. E. Regalado, *Appl. Opt.*, 1988, **27**, 2549–2553.
58 R. T. Graf, J. L. Koenig and H. Ishida, *Appl. Spectrosc.*, 1985, **39**, 405–408.
59 E. D. Palik, *Handbook of optical constants of solids*, Academic Press, 1985.
60 M. Jablan, H. Buljan and M. Soljacic, *Phys. Rev. B: Condens. Matter Mater. Phys.*, 2009, **80**, 245435.
61 I. Pockrand, *Surf. Sci.*, 1978, **72**, 577–588.
62 A. Sinitskii, A. Dimiev, D. V. Kosynkin and J. M. Tour, *ACS Nano*, 2010, **4**, 5405–5413.
63 S. Thongrattanasiri, F. H. L. Koppens and F. Javier Garcia de Abajo, *Phys. Rev. Lett.*, 2012, **108**, 047401.
64 A. Vakil and N. Engheta, *Science*, 2011, **332**, 1291–1294.

65 Z. Q. Li, E. A. Henriksen, Z. Jiang, Z. Hao, M. C. Martin, P. Kim, H. L. Stormer and D. N. Basov, *Nat. Phys.*, 2008, **4**, 532–535.
66 V. P. Gusynin, S. G. Sharapov and J. P. Carbotte, *J. Phys.: Condens. Matter*, 2007, **19**, 026222.
67 H. Yan, Z. Li, X. Li, W. Zhu, P. Avouris and F. Xia, *Nano Lett.*, 2012, **12**, 3766–3771.
68 U. Stoberl, U. Wurstbauer, W. Wegscheider, D. Weiss and J. Eroms, *Appl. Phys. Lett.*, 2008, **93**, 051906.
69 V. P. Verma, S. Das, I. Lahiri and W. Choi, *Appl. Phys. Lett.*, 2010, **96**, 203108.
70 N. Petrone, I. Meric, J. Hone and K. L. Shepard, *Nano Lett.*, 2013, **13**, 121–125.
71 C. L. Nehl, H. W. Liao and J. H. Hafner, *Nano Lett.*, 2006, **6**, 683–688.
72 S. Eustis and M. A. El-Sayed, *J. Appl. Phys.*, 2006, **100**, 044324.
73 T. K. Sarma and A. Chattopadhyay, *Langmuir*, 2004, **20**, 3520–3524.